

Nonlinear Two-Dimensional Quantum Capacitors

Sina Khorasani* and Akshay Koottandavida

École Polytechnique Fédérale de Lausanne, CH-1015, Lausanne, Switzerland

(Dated: September 5, 2022)

Owing to its peculiar energy dispersion, the quantum capacitance property of graphene can be exploited in a two-dimensional layered capacitor configuration with graphene as the electrodes and boron nitride as the insulating dielectric, to obtain a strongly nonlinear behavior at zero bias and small voltages. When the temperature is held sufficiently low, the strong nonlinear interaction emerging from the quantum capacitance can exhibit a diverse range of phenomena. It is expected that the proposed structure could take over the functionalities of nonlinear elements in many cryogenic quantum systems, and in particular, quantum electro-optics. It is shown that ultrastrong coupling may be easily expected with small number of pump photons at temperatures around 1K and capacitor areas of the order of $1\mu\text{m}^2$. As potential applications, we define and discuss a measure of anharmonicity for qubit design, as well as schemes for non-reciprocal devices such as an electromagnetic frequency circulator.

In the field of quantum optomechanics [1–5] and mostly superconducting circuits, it is desirable to have a nonlinear interaction between modes having different frequencies. For this purpose, nanomechanical capacitors [2, 3, 6], kinetic inductors [7, 8], and Josephson junctions [9–13] are mostly used, and in particular for quantum computing [14–16], circuit analogues of quadratic optomechanics [17], and more recently realization of meminductors and memcapacitors [18]. While nanomechanical capacitors effectively appear as third-order nonlinear Kerr elements in the circuits, Josephson junctions, depending on the structure fabrication type and magnetic flux bias, may exhibit various degrees of nonlinear flux/current behavior [19]. The major restriction of Josephson junctions, despite strong nonlinearity, is that they suffer from small current handling capability, which limits the maximum total photon occupation number.

Here, we suggest an alternate solution by proposing the design of a nonlinear quantum capacitance. The capacitor is formed by a graphene-boron nitride-graphene layered, two-dimensional (2D) structure as illustrated in Fig. 1, and has been studied for its optoelectronic properties [20, 21]. Graphene has previously been used in optomechanics as the mechanical element in the form of a drum capacitor [22–24]. But this particular design avoids real physical mechanical motions as the structure is not suspended. In fact, this provides an alternative design for quantum electro-optics [25–27]. Boron nitride (BN), or any other wide-band-gap 2D material, should be a few monolayers thick to prevent tunnel currents, which degrade the performance of the quantum capacitor. The total electrical property of this layered structure is then determined by a geometric parallel-plate capacitor, placed in series with the graphene quantum capacitor. The quantum capacitance at zero bias is divergent and overwhelms the geometric capacitance, in such a way that at zero bias, the nonlinear quantum capacitance would determine the overall behavior. It is shown that this strongly nonlinear feature of quantum capacitance

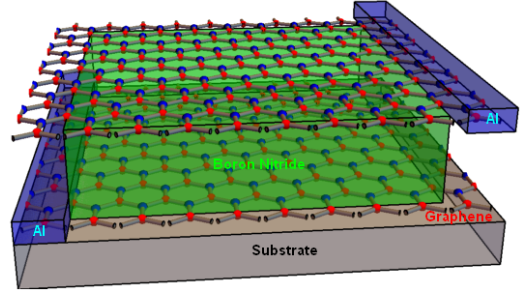


FIG. 1. Schematics of the proposed layered structure.

may be well exploited to obtain an interaction Hamiltonian between multiple electromagnetic modes, with an adjustable interaction rate through electrostatic gating, all the way down to the temperatures around zero. The per-unit capacitance of the 2D layered structure is composed of two components, which arise from geometric and quantum properties. These two appear in series as $C = C_Q || C_G$, where $C_G = \epsilon/t$ is the geometric capacitance per unit area with ϵ and t being the permittivity and thickness of the BN layer, and also $C_Q = \frac{d}{dQ}V$ is the quantum capacitance given per unit area by [28–30]

$$C_Q = \frac{2e^2 k_B T}{\pi(\hbar v_F)^2} \ln \left[2(1 + \cosh \frac{E_F}{k_B T}) \right], \quad (1)$$

where e is the electronic charge, $k_B T$ is the thermal energy, $v_F \approx c/300$ is the Fermi velocity of graphene, and $E_F = eV/2$ is the Fermi energy at either of the graphene electrodes, with V being the external voltage. The typical values of C_Q is in the range of $1 - 10\text{fF}\mu\text{m}^{-2}$ [30]. In the ultralow temperature limit, the above expression approaches the linear form

$$\lim_{T \rightarrow 0} C_Q = \frac{e^3}{\pi(\hbar v_F)^2} |V|. \quad (2)$$

Hence, for the symmetric structure under consideration with $E_F = 0$ at zero bias, we obtain the important re-

sult $C_Q = 0$. The significance of this result is that the overall capacitance of the structure at zero bias and low-voltage is solely determined by its quantum properties. Although being a bit counter-intuitive, this is exactly what one would need to exploit the resulting nonlinear property of the quantum capacitor. Therefore, we obtain the nonlinear charge-voltage relationship

$$Q = \int_0^V C dV = \frac{e^3}{2\pi(\hbar v_F)^2} |V|V, \quad (3)$$

$$U = \int_0^V Q dV = \frac{e^3}{6\pi(\hbar v_F)^2} |V|^3.$$

where $U = \frac{1}{3}\sqrt{2\pi}\hbar v_F \text{sgn}(Q)N^{\frac{3}{2}}$ with $|Q| = eN$ is the total stored energy per unit area. These relations are unfortunately all singular at $V = 0$ and cannot be expanded as polynomial series. But it is possible to proceed directly from (1) for a finite temperature to obtain the series expansions

$$N \approx \frac{2ek_B T}{\pi(\hbar v_F)^2} \left[\ln(2)V + \frac{e^2}{96(k_B T)^2} V^3 + \dots \right], \quad (4)$$

$$U \approx \frac{\pi(\hbar v_F)^2}{2k_B T} \left\{ \frac{N^2}{\ln(16)} - \frac{\pi^2}{4} \left[\frac{\hbar v_F}{\ln(16)k_B T} \right]^4 N^4 + \dots \right\}.$$

Firstly, it is seen from the first expansion term of the second equation, that the linear capacitance per unit area is given as

$$C_0 = \frac{2e^2 k_B T \ln(16)}{\pi(\hbar v_F)^2}. \quad (5)$$

This is to be compared with the geometrical capacitance C_G . The permittivity of BN is $\epsilon = 4.0\epsilon_0$ [20]. Hence taking the dielectric thickness to be $t = 7\text{nm}$, being sufficient to stop tunneling current, gives a geometric capacitance value of $C_G = 5.06\text{fF}\mu\text{m}^{-2}$. At the typical temperature of 1K, we have $C_0 = 0.0563\text{fF}\mu\text{m}^{-2}$, which is much smaller than the geometric capacitance by two orders of magnitude. Hence, our initial assertion to ignore the effect of the geometric capacitance at low temperatures and zero bias is satisfied to a high accuracy. This situation is illustrated in Fig. 2. In general, a dielectric thickness of no less than 2nm should be sufficient to completely disallow tunneling. It could be made thick as long as C_Q dominates by an order of magnitude, yielding the available range of dielectric thickness as $3\text{nm} < t < 70\text{nm}$. Since, the monolayer BN is around only 2.489\AA in thickness [20], t is sufficiently high to warrant an epitaxial growth. Structures of comparable type are being fabricated in integrated optics [31, 32]. In general, there is no reason why other crystalline dielectrics such as SiO_2 or Al_2O_3 could not be used.

Now, suppose that the capacitor is driven by a sinusoidal voltage with angular frequency ω and a fixed phase ϕ . The corresponding charge density operator is given as

$$\hat{Q} = e\hat{N} = \frac{e\psi}{\sqrt{2}}(\hat{a} + \hat{a}^\dagger), \quad (6)$$

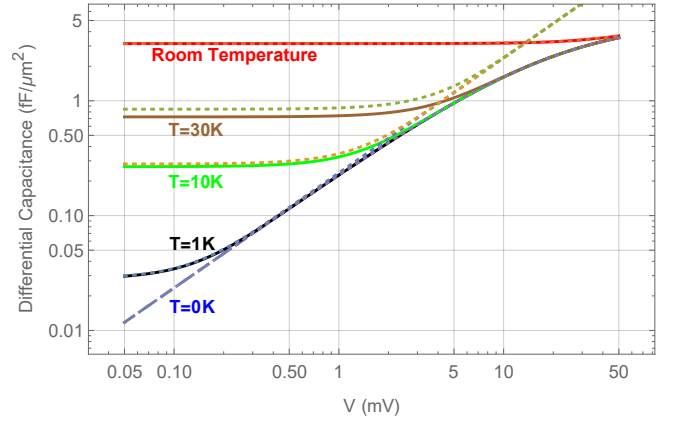


FIG. 2. The differential capacitance of the proposed layered structure at various temperatures on the logarithmic scale. Dashed line is the zero temperature limit. Dotted lines correspond to the quantum capacitance C_Q only, without taking the effect of geometric capacitance C_G into account.

where \hat{a} is the bosonic field operator, satisfying $[\hat{a}, \hat{a}^\dagger] = 1$, and ψ is the fluctuation amplitude of corresponding single-photon number density. Hence, ψ is obtained from (4) as

$$\psi = \sqrt{\frac{k_B T \ln(16)}{2\pi S \hbar v_F^2}} \omega = \chi \sqrt{\omega}. \quad (7)$$

Here, S is the total capacitor area. After adding a resonant inductive term to the Hamiltonian as $\frac{1}{2}L\hat{Q}^2$ with $\hat{Q} = S\hat{Q}$ being the operator of total charge on the 2D quantum capacitor and $\omega = 1/\sqrt{SLC_0}$, this allows us to indicate the Hamiltonian of such a sinusoidal field from (4) as

$$\hat{H} = \hbar\omega \left(\hat{a}^\dagger \hat{a} + \frac{1}{2} \right) - \frac{\hbar\tau}{4} \omega^2 (\hat{a} + \hat{a}^\dagger)^4, \quad (8)$$

where

$$\tau = \frac{\pi^3 S \hbar^5 v_F^6 \chi^4}{2 \ln^4(16) (k_B T)^5} = \frac{\pi \hbar^3 v_F^2}{8 \ln^2(16) S (k_B T)^3}, \quad (9)$$

is a characteristic time constant of nonlinear interaction. Clearly, (8) represents an anharmonic oscillator [14–16] and admits a Kerr-like nonlinearity, and this compares well to that of the Josephson junctions [9–13]. It is not difficult to verify that the range of validity of the anharmonic approximation (9) is limited to $\hbar\omega \approx e|V| < 2k_B T$, which by expressing T in K and frequency in GHz gives the upper photon number limit of $n_{\text{max}} = 41.7T/f$. Hence, at $T = 1\text{K}$ and frequencies in the GHz range, many photons may interact anharmonically. Beyond this value, the 6th order nonlinearity kicks in, which remains valid in the range $4k_B T < e|V| < 6k_B T$, and so on for higher order interactions. Similarly, at sub-Kelvin

temperatures, the usefulness of this nonlinear capacitor may become limited to sub-GHz photons. It should be stressed out that one could access a 3-rd order interaction according to (3) via appropriate DC voltage bias.

It is clear from the above that the nonlinearity is pronounced at small capacitor areas and low temperature. We shall observe that at the typical GHz microwave frequencies and temperatures below 1K this expression easily gives rise to a quite significant Kerr interaction.

Next, we may define a measure of anharmonicity for applications in qubit design [33] as $A = |1 - (\omega_{21}/\omega_{10})| \times 100\%$, where ω_{mn} is the transition frequency between levels m and n . A straightforward calculation gives the estimate $A = 12\tau\omega$. Putting T in K, f in GHz, and S in μm^2 gives $A = 42.85\%f/ST^3$. Using the typical values $T = 1\text{K}$, $f = 4\text{GHz}$, and $S = 100\mu\text{m}^2$ gives an anharmonicity of $A = 1.1714\%$, while at $T = 0.5\text{K}$ we obtain $A = 13.71\%$, being sufficiently large for qubit applications.

In a similar manner, for a multi-mode field composed of a few sinusoidal terms and by adding resonant inductive terms as $\frac{1}{2}\sum L_n \hat{q}_n^2$ with $\hat{q}_n = S\hat{Q}_n$ and $\omega_n = 1/\sqrt{SL_n C_0}$, we may write down the total Hamiltonian

$$\hat{H} = \hbar \sum_n \omega_n \left(\hat{a}_n^\dagger \hat{a}_n + \frac{1}{2} \right) - \frac{\hbar\tau}{4} \left[\sum_n \sqrt{\omega_n} (\hat{a}_n + \hat{a}_n^\dagger) \right]^4. \quad (10)$$

Here, we have the usual commutation rules between individual field operators as $[\hat{a}_n, \hat{a}_m^\dagger] = \delta_{nm}$ and $[\hat{a}_n, \hat{a}_m] = 0$. Now, we limit the discussion to only three modes, where the interacting \mathbb{H} and non-interacting \hat{H}_0 terms may be separated as $\hat{H} = \hat{H}_0 - \mathbb{H}$ to yield the three basic types of interactions in the Hamiltonian

$$\mathbb{H} = \mathbb{H}^{(1)} + \mathbb{H}^{(2)} + \mathbb{H}^{(3)}, \quad (11)$$

with

$$\mathbb{H}^{(1)} = \frac{1}{2} \sum_{n \neq m} \hbar \gamma_{nmm} (\hat{a}_n + \hat{a}_n^\dagger)^2 (\hat{a}_m + \hat{a}_m^\dagger)^2, \quad (12)$$

$$\mathbb{H}^{(2)} = \frac{3}{2} \sum_{n \neq m} \hbar \gamma_{nmm} (\hat{a}_n + \hat{a}_n^\dagger)^3 (\hat{a}_m + \hat{a}_m^\dagger),$$

$$\mathbb{H}^{(3)} = \frac{3}{2} \sum_{n \neq m \neq l} \hbar \gamma_{nml} (\hat{a}_n + \hat{a}_n^\dagger)^2 (\hat{a}_m + \hat{a}_m^\dagger) (\hat{a}_l + \hat{a}_l^\dagger).$$

Here, $\gamma_{nml} = \tau \omega_n \sqrt{\omega_m \omega_l}$.

We can suppose that the interaction is driven at mode 0 with a strong coherent field and frequency $\Omega = \omega_0$, in such a way that $\hat{a}_0 \rightarrow \bar{a} + \delta\hat{a}$. Neglecting beyond simple nonlinear interactions between modes 1 and 2, and with three modes interacting, only $\mathbb{H}^{(3)}$ contributes significantly. Then, we obtain

$$\mathbb{H} = \hbar \bar{G} (\hat{a}_1 + \hat{a}_1^\dagger) (\hat{a}_2 + \hat{a}_2^\dagger), \quad (13)$$

where $\bar{G} = 3\gamma_{012}(\bar{a} + \bar{a}^*)^2$.

Now we use the Rotating Wave Approximation (RWA) and neglect the counter-rotating terms, to obtain the remaining significant interactions. The RWA approximation is not valid in general, and in some cases, the counter-rotating terms have been shown to have a considerable effect on the evolution of system [34, 35]. Such a Hamiltonian has been achieved in systems using Josephson junction [47] and extended to realise non-reciprocal devices [46]. Anyhow, by application of RWA one may distinguish two particular resonant cases with $2\Omega = \omega_1 \pm \omega_2$, for which the interaction Hamiltonian (11) greatly simplifies and takes either of the forms

$$\mathbb{H} \approx \hbar G (e^{2j\theta} \hat{a}_1 \hat{a}_2^\dagger + e^{-2j\theta} \hat{a}_1^\dagger \hat{a}_2), \quad (14)$$

for $2\Omega = \omega_1 - \omega_2$ and

$$\mathbb{H} \approx \hbar G (e^{2j\theta} \hat{a}_1^\dagger \hat{a}_2^\dagger + e^{-2j\theta} \hat{a}_1 \hat{a}_2), \quad (15)$$

for $2\Omega = \omega_1 + \omega_2$. Also, $G = g_0 |\bar{a}|^2 = 3\gamma_{012} |\bar{a}|^2$ is the overall interaction rate and $\theta = \angle \bar{a}$ is the phase of the coherent drive.

On one hand, by choice of $2\Omega = \omega_1 - \omega_2$ and the Hamiltonian (14), one may achieve a beam-splitter or hopping interaction, where the mode at frequency Ω is pumped strongly by a coherent field. This type of interaction can facilitate, for example, a non-reciprocal response between the modes under the appropriate conditions [44, 48].

On the other hand, by choice of $2\Omega = \omega_1 + \omega_2$ and the Hamiltonian (15), one may achieve the parametric amplifier interaction. We can set up a system, similar to that discussed in [46], in order to realise a directional amplifier. However, the coupling is mediated by the quantum capacitor, as opposed to a Josephson junction, which in principle requires a magnetic bias to induce the third order interaction in the system.

It is possible to estimate the interaction from the above relations for G . Expressing the temperature T in K, capacitor area S in μm^2 , and drive frequency $f = \Omega/2\pi$, electromagnetic frequencies $f_n = \omega_n/2\pi$ and also the single-photon interaction rate g_0 in GHz, we obtain

$$g_0 = 2\pi \times 0.143 \frac{f \sqrt{f_1 f_2}}{ST^3}. \quad (16)$$

As an example, taking $S = 100\mu\text{m}^2$ at $T = 1\text{K}$, with $f = 4\text{GHz}$, $f_1 = 2\text{GHz}$, and $f_2 = 10\text{GHz}$ satisfies the resonance condition for the hopping interaction (14). This gives a linear capacitance value of $C_0 = 5.63\text{fF}$ and also makes it possible to calculate the values of corresponding tank inductors and external circuitry. For these values, the single-photon interaction rate is $g_0 = 2\pi \times 25.55\text{MHz}$. This fairly well falls into the domain of strong coupling. The same value at the temperature of $T = 4\text{K}$ is severely degraded to the weakly coupled value $g_0 = 2\pi \times 399.2\text{kHz}$, while at the lower temperature of $T = 0.25\text{K}$, it is significantly enhanced to $g_0 = 2\pi \times 1.635\text{GHz}$, which is of course ultrastrongly coupled. Hence, it is very easy to

obtain extremely strong single-photon nonlinear interaction rates even with low pump levels, without need to dilution refrigerators.

Other issues to be considered here is the superconductor contact to the graphene electrodes, as well as the charging time of the capacitor. The first issue brings up the proximity effect, while the second is related to the intrinsic conductivity of the graphene. The proximity effect has been well studied [36–39]. It has been experimentally and theoretically established that in graphene, the finite normal state conductance can maintain finite supercurrent, even at zero bias. Hence, the electrical current should have no problem flowing freely through graphene electrodes. Moreover, it is well known that carriers in graphene are essentially ballistic [40, 41] at low temperatures over distances of a few microns.

Next, we may turn to the issue of charging delay. Remarkably, at zero bias, the steady state charge density of graphene is also expected to be zero, which should admit no normal state conductance, but it is well known also that the conductance of graphene at zero bias is also nonzero and finite, being in fact equal to the quantum conductance $\sigma_Q = 2e^2/\pi\hbar$ [39, 42, 43].

In that sense, the ratio of quantum capacitance to quantum conductance with the unit of time, is simply proportional to the Fermi energy

$$\tau_Q = \frac{C_Q}{\sigma_Q} = \frac{|E_F|}{\hbar v_F^2}. \quad (17)$$

The time-constant τ_Q determines the quantum characteristic time for charge/discharge of capacitor when the current is supplied in the Ohmic regime. Not only for the structure under consideration, it approaches zero at zero bias, but also the electric current is mainly non-Ohmic and dissipation-free over distances of the order of few microns, since charges move almost ballistically across graphene electrodes. So, it should be safe to ignore both of these aspects in a precisely fabricated 2D layered structure, as long as it is void of defects and interfaces are atomically flat.

Now, as potential applications, we discuss schemes for two non-reciprocal devices. Assume that initially we have three electromagnetic modes with frequencies ω_1 , ω_2 , and ω_3 , mutually coupled via three nonlinear 2D capacitors, interacting through the Hamiltonian described in (14). We set up the hopping interaction between each of the 3 modes using the scheme mentioned previously. Hence the Hamiltonian of the system could be written as $\mathbb{H} = \mathbb{H}_{12} + \mathbb{H}_{23} + \mathbb{H}_{31}$, where

$$\begin{aligned} \mathbb{H}_{12} &= \hbar g_3 (e^{i\phi_3} \hat{a}_1 \hat{a}_2^\dagger + e^{-i\phi_3} \hat{a}_1^\dagger \hat{a}_2), \\ \mathbb{H}_{23} &= \hbar g_1 (e^{i\phi_1} \hat{a}_2 \hat{a}_3^\dagger + e^{-i\phi_1} \hat{a}_2^\dagger \hat{a}_3), \\ \mathbb{H}_{31} &= \hbar g_2 (e^{i\phi_2} \hat{a}_3 \hat{a}_1^\dagger + e^{-i\phi_2} \hat{a}_3^\dagger \hat{a}_1). \end{aligned} \quad (18)$$

A probe signal (input) at, say mode 1, has two pathways for conversion to mode 3 ($1 \rightarrow 2 : 2 \rightarrow 3$ or $1 \rightarrow 3$). The

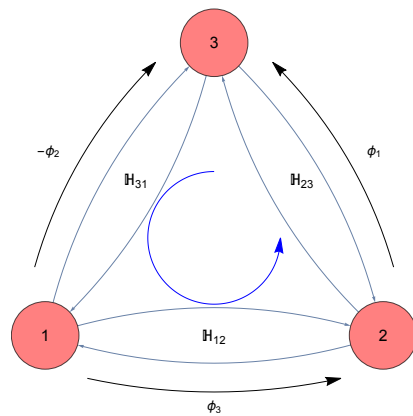


FIG. 3. The mode coupling scheme in an ideal circulator. The signal can take two pathways for conversion from, say, mode 1 to mode 3. The phase difference between the two paths, $\Delta\phi$, can be controlled and by setting $\Delta\phi = \pm\frac{\pi}{2}$ provides the condition for interference between the paths. Hence only one pathway is preferred (say, anti-clockwise, blue curve) and not the opposite (clockwise) for mode conversion. In this scheme, any one of the 3 modes can be taken as the input while any of the other two may play the role of output.

signal picks up different phases while traversing through these two paths [45]. The phase difference at mode 3 (output) is $\Delta\phi = \phi_1 + \phi_3 - \phi_2$ (Fig. 3). By controlling the phases of the pumps, one can set $\Delta\phi = \pm\frac{\pi}{2}$, thereby allowing interference between the two paths. This results in the signal propagating only in one of the two paths, hence breaking the symmetry of the system. Hence we realise an ideal circulator. Using the quantum Langevin equation in the RWA and input-output formalism [2, 49, 50], one can write the equations of motion, and hence the Langevin matrix of the system as

$$\mathbf{M} = \begin{bmatrix} -(i\omega_1 + \frac{\kappa_1}{2}) & -ig_3 e^{-i\phi_3} & -ig_2 e^{i\phi_2} \\ -ig_3 e^{i\phi_3} & -(i\omega_2 + \frac{\kappa_2}{2}) & -ig_1 e^{-i\phi_1} \\ -ig_3 e^{-i\phi_2} & -ig_2 e^{i\phi_1} & -(i\omega_3 + \frac{\kappa_3}{2}) \end{bmatrix}, \quad (19)$$

where κ_i is the decay rate of the i -th mode. We see that \mathbf{M} is not symmetric about the diagonal. In order to see the non-reciprocal response, one can solve the above system in the Fourier space, obtaining the scattering matrix \mathbf{S} that relates the input signal to the mode converted output signal as $\hat{a}_{out} = \mathbf{S} \hat{a}_{in}$. By tuning the parameters, it is clear from the ratio of scattering amplitudes that symmetry of the system has indeed been broken (Fig. 4).

Physically, in the two schemes discussed above, $\Delta\phi$ acts as an artificial gauge flux and plays the role of the magnetic field in a conventional circulator [46]. The lack of an external magnetic bias is advantageous in situations such as qubit read-out schemes, where the performance is severely hindered by the unwanted noises that enter the system through various ports. Hence such a scheme could be a precursor to devices which achieve non-reciprocity

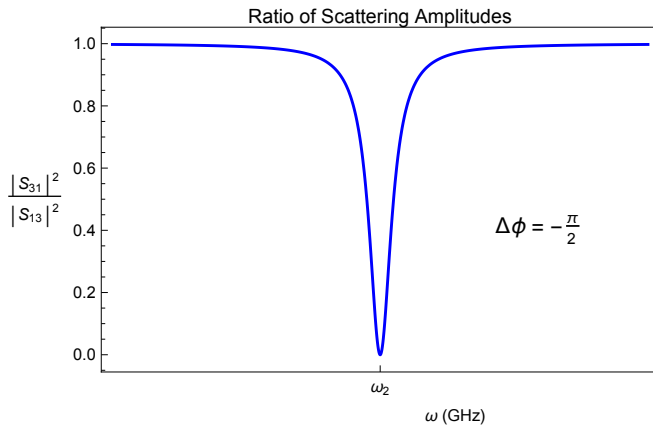


FIG. 4. The ratio of between $1 \rightarrow 3$ and $3 \rightarrow 1$ mode conversion scattering amplitudes. Due to destructive interference, set up by the phase difference parameter, the symmetry of the system is broken.

between such physical ports of the system.

In summary, we have shown that a layered 2D quantum capacitor with graphene electrodes is highly nonlinear, if temperature is held sufficiently low and there is no bias. All requirements were shown to be met at microwave (GHz) frequencies, temperatures of the order of 1K, and capacitors as small as a few μm^2 . We showed that under the correct choice of strong pump and weak fields, the interaction Hamiltonian would be that of a beam splitter with adjustable phase from the pump, depending on the resonance condition. Potential applications were discussed and it was shown that the interaction could be easily forced into the ultrastrong regime. It is anticipated that this proposal would open up a new highway in the field of quantum microwave electro-optics, while allowing access to interaction rates which are not easily achievable through other methods. The high strength of Kerr nonlinearity makes the proposed quantum capacitor potentially very useful for design of novel charge quantum bits as well.

* sina.khorasani@epfl.ch

- [1] T. J. Kippenberg, K. J. Vahala, *Science* **321**, 1172 (2008).
- [2] M. Aspelmeyer, T. Kippenberg, F. Marquardt, *Cavity Optomechanics* (Springer, Berlin, 2014).
- [3] M. Aspelmeyer, T. J. Kippenberg, F. Marquardt, *Rev. Mod. Phys.* **86**, 1391 (2014).
- [4] F. Marquardt, S. M. Girvin, *Physics* **2**, 40 (2009).
- [5] P. Meystre, *Ann. Phys.* **525**, 215 (2013).
- [6] L. D. Tóth *et al.*, arxiv: 1602.05180 (2016).
- [7] S. Salahuddin, M. Lundstrom, *IEEE Trans. Electron*

- Dev.* **52**, 1734 (2005).
- [8] A. J. Annunziata *et al.*, *Nanotechnology* **21**, 445202 (2010).
- [9] M. A. Sillanpää *et al.*, *Phys. Rev. Lett.* **95**, 206806 (2005).
- [10] J.-M. Pirkkalainen *et al.*, *Nat. Commun.* **6**, 6981 (2015).
- [11] R. Barends *et al.*, *Nature* **534**, 222 (2016).
- [12] V. A. Oboznov *et al.*, *Phys. Rev. Lett.* **96**, 197003 (2006).
- [13] A. K. Feofanov *et al.*, *Nat. Phys.* **6**, 593 (2010).
- [14] J. Q. You, F. Nori, *Nature* **474**, 589 (2011).
- [15] I. M. Georgescu, S. Ashhab, F. Nori, *Rev. Mod. Phys.* **86**, 153 (2014).
- [16] Z.-L. Xiang *et al.*, *Rev. Mod. Phys.* **85**, 623 (2013).
- [17] E.-J. Kim, J. R. Johansson, F. Nori, *Phys. Rev. A* **91**, 033835 (2015).
- [18] S. N. Shevchenko, Y. V. Pershin, F. Nori, *Phys. Rev. Appl.* **6**, 014006 (2016).
- [19] K. K. Likharev, *Dynamics of Josephson Junctions and Circuits* (Gordon and Breach, Amsterdam, 1983).
- [20] S. Khorasani, *IEEE J. Quantum Electron.* **50**, 307 (2014).
- [21] C. Palacios-Berraquero *et al.*, *Nat. Commun.* **7**, 12978 (2016).
- [22] X. Song *et al.*, *Phys. Rev. Lett.* **113**, 027404 (2014).
- [23] V. Singh *et al.*, *Phys. Rev. B* **93**, 245407 (2016).
- [24] R. M. Cole *et al.*, *Phys. Rev. Applied* **3**, 024004 (2015).
- [25] V. Caprara Vivoli *et al.*, *Phys. Rev. Lett.* **116**, 070405 (2016).
- [26] M. Tsang, *Phys. Rev. A* **81**, 063837 (2010).
- [27] M. Tsang, *Phys. Rev. A* **84**, 043845 (2011).
- [28] S. Dröscher *et al.*, *Appl. Phys. Lett.* **96**, 152104 (2010).
- [29] T. Fang *et al.*, *Appl. Phys. Lett.* **91**, 092109 (2007).
- [30] J. Xia *et al.*, *Nat. Nanotech.* **4**, 505 (2009).
- [31] C. T. Phare *et al.*, *Nat. Photon.* **9**, 511 (2015).
- [32] Z. Sun, A. Martinez, F. Wang, *Nat. Photon.* **10**, 227 (2016).
- [33] J. Clarke, F. K. Wilhelm, *Nature* **453**, 1031 (2008).
- [34] M. Alidoosty, S. Khorasani, M. H. Aram, *IEEE J. Quantum Electron.* **49**, 1066 (2013).
- [35] D. Malz, A. Nunnenkamp, arxiv: 1610.00154 (2016).
- [36] H. B. Heersche *et al.*, *Nature* **446**, 56 (2007).
- [37] C. Ojeda-Aristizabal *et al.*, *Phys. Rev. B* **79**, 165436 (2009).
- [38] K. Komatsu *et al.*, *Phys. Rev. B* **86**, 115412 (2012).
- [39] C. Li *et al.*, *Phys. Rev. B* **94**, 115405 (2016).
- [40] Y. P. Bliokh, V. Freilikher, F. Nori, *Phys. Rev. B* **87**, 245134 (2013).
- [41] A. V. Rozhkov *et al.*, *Phys. Rep.* **648** 1 (2016).
- [42] T. C. Li, S.-P. Lu, *Phys. Rev. B* **77**, 085408 (2008).
- [43] N. Tombros *et al.*, *Nat. Phys.* **7**, 697 (2011).
- [44] A. Metelmann, A.A. Clerk, *Phys. Rev. X* **5**, 021025 (2015).
- [45] L. Ranzani, J. Aumentado, *New J. Phys.* **17** 023024 (2015).
- [46] K. M. Sliwa *et al.*, *Phys. Rev. X* **5**, 041020 (2015).
- [47] B. Abdo, A. Kamal, M. H. Devoret, *Phys. Rev. B* **87**, 014508 (2013).
- [48] A. Nunnenkamp *et al.*, *Phys. Rev. Lett.* **113**, 023604 (2014).
- [49] C. W. Gardiner, M. J. Collett, *Phys. Rev. A* **31**, 6 (1985).
- [50] A. A. Clerk *et al.*, *Rev. Mod. Phys.* **82**, 1155 (2010).